



ChemComm

**A cobalt–manganese layered oxide/graphene composite as
an outstanding oxygen evolution reaction electrocatalyst**

Journal:	<i>ChemComm</i>
Manuscript ID	CC-COM-06-2021-003152.R1
Article Type:	Communication

SCHOLARONE™
Manuscripts



Journal Name

COMMUNICATION

A cobalt–manganese layered oxide/graphene composite as an outstanding oxygen evolution reaction electrocatalyst

Hiroaki Kobayashi,^{‡a,*} Yuuki Sugawara,^{‡b,*} Takeo Yamaguchi,^b and Itaru Honma^aReceived 00th January 20xx,
Accepted 00th January 20xx

DOI: 10.1039/x0xx00000x

www.rsc.org/

To enhance the oxygen evolution reaction mass activity of cobalt–manganese layered oxide (CMO), we develop a one-pot synthetic process to anchor CMO onto graphene sheets (CMO/G). Its mass activity is 66-fold higher than that of physically mixed bare CMO with graphene and even better than those of previously reported graphene-supported first-row transition metal oxide-based electrocatalysts. The remarkable mass activity is attributed to the excellent intrinsic activity of CMO, small and well-dispersed CMO nanosheets on graphene sheets and hydrophilized graphene by the synthetic process. Further, CMO/G exhibits excellent stability.

The depletion of fossil fuels and the issues of global warming and air pollution have considerably stimulated the development of alternative sustainable energy supply systems. Hydrogen is considered an ideal energy carrier with high energy density and eco-friendliness. Electrochemical water splitting is a promising sustainable process that can convert electricity from renewable energy resources, such as wind and solar power, to pure hydrogen using abundant water resources without carbon emissions. However, the anodic oxygen evolution reaction (OER: $4\text{OH}^- \rightarrow \text{O}_2 + 2\text{H}_2\text{O} + 4\text{e}^-$) in water splitting has a large overpotential,¹ and it is a serious concern for practical use. Ruthenium- and iridium-based compounds possess prominent catalytic activities for the OER,² but their high costs and scarcity limit their widespread application. Hence, nonprecious electrocatalysts with low cost and excellent OER activities have been increasingly sought.

First-row transition metals, such as Mn, Fe, Co and Ni, have received considerable interest as alternative OER electrocatalysts because of their earth abundance and cost-effectiveness.³ In particular, metal oxide-based electrocatalysts

have attracted much attention due to their beneficial advantages, such as easy synthesis, low toxicity and high electrochemical activities. Many scholars have attempted to develop prominent multimetallic oxide-based OER electrocatalysts comprising first-row transition metals and manipulated their OER performance by rendering their elemental compositions.⁴ Recently, we reported an outstanding OER electrocatalyst, CaFe_2O_4 ,⁵ which can be easily prepared *via* the malic acid-aided sol–gel method.⁶ We highlighted that the OER activity of CaFe_2O_4 was much higher than those of other Fe-based oxides containing alkaline- or rare-earth metals, even surpassing the benchmark IrO_2 .⁵ Further, the geometrical arrangements of metal oxides highly affect their OER activities.⁷ We recently demonstrated that Co–Mn binary oxides bearing layered-type structures, denoted as CMO, exhibited much higher intrinsic OER activity than spinel and tunnel structures. The superior OER activity of layered CMO resulted from its larger Co–metal coordination number. The OER activity of CMO is high compared with previously reported first-row transition metal-based bimetallic oxides.⁸

The activities of electrocatalysts are generally compared using specific activity and mass activity. The former measure is defined as a catalytic current normalized by the surface area of catalyst particles and reflects the intrinsic activity of the catalyst. It does not depend on particle size. Meanwhile, the latter measure is defined as a catalytic current normalized by the loading mass of the catalyst and is more significant for practical implementation in terms of cost. It is strongly affected by particle size because larger particles have smaller surface areas, *i.e.*, fewer active sites per mass. The abovementioned CMO exhibited prominent OER specific activity, but had low mass activity because the reported synthetic process for CMO could only fabricate large nanoparticles with sizes in the range of 200–300 nm; therefore, it is necessary to develop a novel synthetic methodology for fabricating CMO with smaller particle diameters to improve OER mass activity for widespread use.

^a Institute of Multidisciplinary Research for Advanced Materials, Tohoku University, 2-1-1 Katahira, Aoba-ku, Sendai, Miyagi 980-8577, Japan

^b Laboratory for Chemistry and Life Science, Institute of Innovative Research, Tokyo Institute of Technology, R1-17, 4259 Nagatsuta-cho, Midori-ku, Yokohama, Kanagawa 226-8503, Japan.

[†] Electronic Supplementary Information (ESI) available: Detailed experimental procedures; Supplementary data. See DOI: 10.1039/x0xx00000x

[‡] H.K. and Y.S. contributed equally to this work.

To decrease the size of catalyst nanoparticles and improve their catalytic performance, coupling with well-ordered conductive carbon supports, such as graphene sheets is an efficient strategy to boost electrocatalytic reactions because of the high electrical conductivity, large surface area and good mechanical strength of graphene.⁹ Several researchers have directly anchored metal oxide catalysts to graphene supports *via* two-step or one-pot synthesis and demonstrated their high OER performance. For instance, MnCo_2O_4 ,^{9b} NiCo_2O_4 ,¹⁰ FeCo_2O_x ,¹¹ CoFe_2O_4 ,¹² NiMnCoO_x ,¹³ $\text{Co/CoFe}_2\text{O}_4$ ¹⁴ and CoNi-MOF^{15} were directly grown on graphene surface or its derivatives *via* one-pot synthesis; consequently, the nanoparticles had a size of less than 100 nm and demonstrated excellent OER mass activities.

In this study, to significantly enhance the OER mass activity of CMO, we develop a one-pot synthetic process to directly anchor CMO onto a graphene sheet, which is denoted as CMO/G. Fig. 1a illustrates the synthetic scheme of CMO/G. This synthetic process is based on a one-pot reduction reaction of metal cations on graphene. The well-defined layer structure of CMO is constructed *via* hydration of Co^{2+} by controlling the amount of water in the reaction mixture. The obtained CMO/G was characterized, and its OER mass activity was evaluated and compared with bare CMO and previously reported bimetallic oxide-based OER electrocatalysts.

The CMO/G composite was successfully prepared through the modified procedure of CMO by dispersing graphene nanopowders into the reaction solution (Fig. 1a).⁸ A transmission electron microscopy (TEM) image (Fig. 1b) displays a sheet structure with wrinkles and shaded areas. The wrinkles derive from the graphene sheet, whereas the shaded areas indicate the deposition of CMO on the graphene sheet. Fig. 1c depicts the selected area electron diffraction (SAED), obtained from Fig. 1b, which shows Debye–Scherrer rings attributable to CMO ($d = 0.24$ and 0.14 , see Fig. S2 in the ESI) and graphene ($d = 0.21$ and 0.12 , attributable to the 010 and 110 diffractions of graphite [ICSD collection code: 76767]), respectively, supporting CMO and graphene composition. X-ray diffraction patterns of CMO/G (Fig. S1) also supported the composite formation. In addition, a high-resolution TEM (HR-TEM) of the

shaded part (inset of Fig. 1b) shows a clear lattice fringe of 0.69 nm; the same fringe was observed in bare CMO (Fig. S2). The sheet/particle diameters of CMO/G and bare CMO are listed in Table S1. The diameters of CMO in CMO/G ranged from 40 to 80 nm, and the nanosheets were well dispersed on graphene. Moreover, bare CMO exhibited much larger particles with sizes in the range of 200 – 300 nm, which were densely aggregated (Fig. S2). The size difference suggested that CMO in CMO/G possessed a larger number of active sites per mass than bare CMO. Further, carbon, hydrogen and nitrogen elemental analysis indicated that CMO/G contained CMO and graphene with a $59:41$ weight ratio. The valence state of Co in CMO/G estimated from X-ray photoelectron spectroscopy was $3+$, and that of Mn was between $3+$ and $4+$ (Fig. S3). According to the reported inferior OER activity of Mn to that of Co in a Co–Mn bimetal oxide¹⁶ and low intrinsic OER activity of the layered structure with MnO_6 octahedra connection,¹⁷ Co is expected to be a major active site in CMO/G.

The OER performance of CMO/G and physically mixed bare CMO and graphene (denoted as CMO+G_PM) was evaluated by cyclic voltammetry scans in O_2 -saturated 1 M KOH using a rotating disk electrode (RDE) at a rotating rate of 1600 rpm (Fig. S4). Fig. S5a represents the iR -corrected OER polarization curves. The OER overpotentials of CMO/G and CMO+G_PM versus the theoretical value for the OER (1.23 V vs. RHE) at a current density of 10 $\text{mA cm}^{-2}_{\text{disk}}$ were 0.36 and 0.43 V, respectively. In addition, Tafel slopes (Fig. S5b) estimated from Fig. S5a also indicated favourable OER kinetics for CMO/G. To fairly compare the practical OER performance of CMO/G and CMO+G_PM, we calculated the OER mass activities by normalizing the OER currents using the loading amounts of metal oxides per RDE disk. Their OER mass activities are displayed along with those of bare CMO and pristine graphene in Fig. 2a; CMO/G exhibited much higher OER mass activity than CMO+G_PM, CMO and graphene. CMO had insufficient electrical conductivity, which prevented the electron transport from active sites to an electrode, and graphene did not intrinsically catalyze OER. Notably, the mass activity of CMO/G

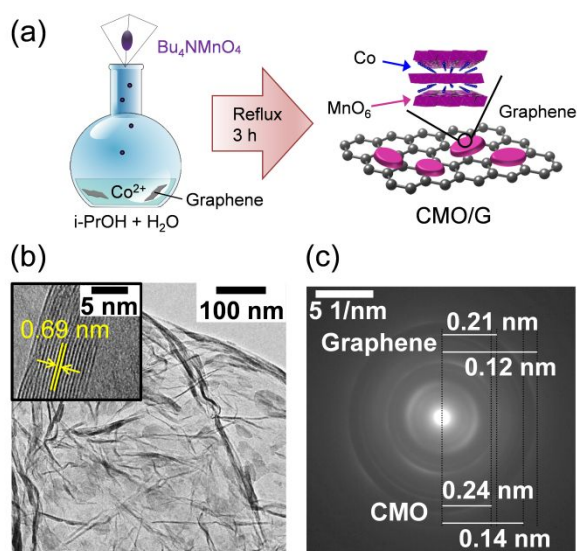


Fig. 1 (a) Schematic illustration of the reaction procedure. (b) TEM and (c) SAED images of CMO/G.

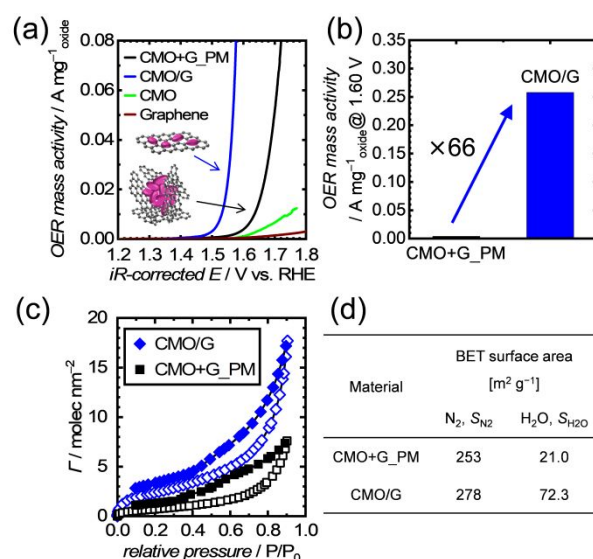


Fig. 2 (a) OER polarization curves CMO+G_PM, CMO/G, bare CMO and pristine graphene with an electrode rotating rate of 1600 rpm in O_2 -saturated 1 M KOH. (b) Mass activities of CMO+G_PM and CMO/G at 1.60 V. (c) H_2O adsorption-desorption isotherms. (d) BET surface area of CMO+G_PM and CMO/G.

at 1.60 V was 66-fold higher than that of CMO+G_PM (Fig. 2b). In addition, electrochemical impedance spectroscopy (EIS) was performed. Fig. S6 shows the collected Nyquist plots from EIS, and they were fitted using a basic equivalent circuit (Fig. S7) to estimate the charge-transfer resistance (R_{ct}). R_{ct} for CMO/G was 30 Ω , much smaller than that of CMO+G_PM (250 Ω), indicating that CMO/G promoted better OER kinetics than CMO+G_PM. The significant improvement of OER mass activity for CMO/G was ascribed to the more hydrophilic behaviour, the much smaller sheet diameter and better interfacial contact of CMO/G than bare CMO, which can be obtained through the developed synthetic process. During the reduction of MnO_4^- , it can partially oxidize hydrophobic graphene and hydrophilize its surface. Fig. 2c and d show H_2O adsorption–desorption isotherms and Brunauer–Emmett–Teller (BET) surface areas with N_2 (S_{N_2}) and H_2O (S_{H_2O}) adsorbents. CMO/G adsorbs more H_2O than CMO+G_PM, although S_{N_2} exhibited similar values. In fact, the S_{H_2O}/S_{N_2} ratio of CMO/G was 0.260, approximately three times higher than that of CMO+G_PM ($S_{H_2O}/S_{N_2} = 0.0830$). Further, the contact angles on the CMO+G_PM and CMO/G surfaces over glassy carbon substrates were $158 \pm 4.09^\circ$ and $147 \pm 6.90^\circ$ (Fig. S8), respectively, which also indicated that graphene was rendered for more hydrophilicity during the synthetic process of CMO/G. The hydrophilicity of a catalyst surface is a critical factor for high OER electrocatalytic activity because a hydrophilic surface can increase the wettability of electrodes to an electrolyte solution, which inhibits the coalescence of evolved O_2 bubbles and accelerates the efficient release of the bubbles from electrodes and the mass transfer of electrolytes, including reactants, to active sites.¹⁸ In addition, the hydrophilization of graphene surface can suppress graphene sheet restacking according to the similar values of S_{N_2} for CMO+G_PM and CMO/G (Fig. 2d), which is also preferable to retain accessible active sites. Therefore, the partial oxidation of hydrophobic graphene by the one-pot process renders the CMO/G composite more hydrophilic, thereby making it highly OER active. Further, the process resulted in small CMO sheet diameters, *i.e.*, 40–80 nm, with good dispersion on graphene (Fig. 1b). In contrast, bare CMO nanoparticles possessed much larger diameters in the 200–300 nm range and exhibited dense aggregation (Fig. S2). Moreover, the process resulted in good interfacial contacts between CMO nanosheets and graphene sheets, which can reduce the grain boundary resistance and was beneficial for electrochemical reactions. On the other hand, a physical mixing of CMO and graphene to prepare CMO+G_PM caused a large grain boundary resistance.¹⁹

Further, when comparing CMO/G with previously reported multimetallic oxide-based OER electrocatalysts, its OER mass activity was superior to those of any previously reported oxide-based OER electrocatalysts bearing nonprecious first-row transition metals mixed with carbon materials (Table S2). Remarkably, CMO/G exhibited better OER mass activity than any previously reported first-row transition metal oxide-based OER electrocatalyst supported on graphene derivatives through one-pot synthesis (Fig. 3 and Table S3).^{9b,12,13,20} The examination of the OER mass activities demonstrated that CMO/G is a promising OER electrocatalyst that can generate a large OER

current despite its small loading amounts on electrodes. The outstanding OER mass activity of CMO/G was attributed to the following features: (i) the layered-type CMO exhibited superior specific activity to most bimetallic oxides bearing first-row transition metals, *e.g.*, spinel oxides, which induced the high catalytic performance per surface area of catalyst particles without a diffusion issue of electrolyte ions; (ii) the developed one-pot synthetic process enabled the fabrication of smaller deposited nanosheets on graphene sheets, which resulted in a large specific surface area; (iii) the synthetic process hydrophilized graphene during the reaction and then increased the electrode surface wettability. Therefore, CMO/G showed outstanding mass activity, exhibiting an advantage in terms of cost.

Moreover, long-term durability is another crucial point for practical use. The durability test of CMO/G was performed by repeating potential cycles for the OER region in 1 M KOH because this method can relatively suppress erroneous activity decays by an accumulation of microscopic O_2 bubbles over active sites compared with chronoamperometry.²¹ OER polarization curves before and after potential cycles are shown in Fig. 4a, demonstrating that the OER current at a higher potential slightly decreased after 1000 cycles because of a little corrosion of conductive graphene support, whereas the OER current at lower potential was even unchanged after 1000



Fig. 3 OER mass activities of the previously reported multimetallic oxides-based electrocatalysts containing first-row transition metals coupled with graphene derivatives. The mass activities were calculated by measured currents at 1.60 V in OER polarization curves and loading amount of oxide on RDE. rGO: reduced graphene oxide; N-G: nitrogen-doped graphene; N-rGO: nitrogen-doped reduced graphene oxide.

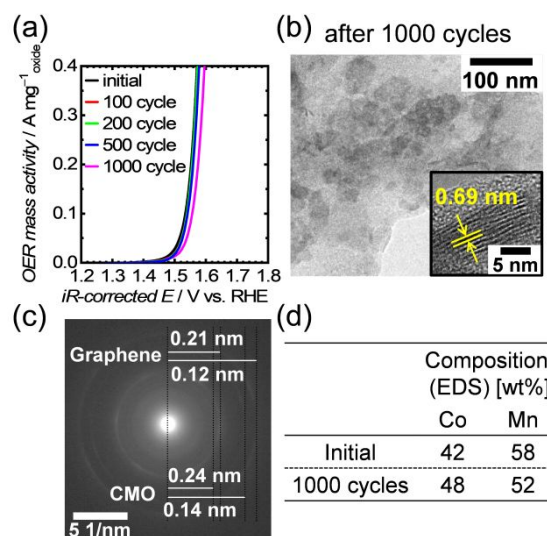


Fig. 4 (a) OER polarization curves of CMO/G at an electrode rotating rate of 1600 rpm in N_2 -saturated 1 M KOH. (b) TEM and (c) SAED images of the CMO/G after 1000 cycles. (d) Elemental ratio of Co and Mn in the CMO/G before and after 1000 cycles.

cycles, which suggested that the catalytic activity of CMO did not decay. Fig. 4b depicts TEM images of CMO/G after 1000 cycles, indicating that graphene wrinkles disappeared by potential cycles, which also supported graphene partial corrosion under high potential in the OER. Nevertheless, the aged CMO nanosheets on graphene retained their sheet size and density. The results indicated that the nanosheets neither aggregated with each other nor detached from graphene during the durability test. In addition, a lattice fringe of 0.69 nm was retained after 1000 cycles (Fig. 4b [inset]); consistent with the as-synthesized CMO/G. Fig. 4c displays the SAED image of CMO/G after 1000 cycles. The diffraction patterns of CMO and graphene agreed well with those of the as-synthesized CMO/G (Fig. 1c), which confirmed that the structures of CMO and graphene were significantly retained. Further, Fig. 4d depicts the result of energy-dispersive X-ray spectroscopy analysis before and after 1000 cycles and highlights that the CMO nanosheets possess Co and Mn elemental contents similar to those of the initial sheets, thereby indicating the high stability of CMO/G during the OER measurement in alkaline media. Because of the high stability of CMO/G, its OER activity after long-term potential cycling remarkably exceeded that of the benchmark IrO₂ (Fig. S9). Thus, the results demonstrated that CMO/G is a promising candidate for an active and durable OER electrocatalyst for practical use.

In conclusion, we developed a novel one-pot synthetic methodology to yield small and well-dispersed nanosheets of layered-type CMO deposited on hydrophilized graphene sheets. The synthesized CMO/G showed excellent OER mass activity in alkaline media, exceeding those of any previously reported first-row transition metal-based oxides supported on graphene derivatives through one-pot synthesis. In addition, CMO/G exhibited excellent durability during long-term OER measurement. Hence, CMO/G is highly promising as an OER electrocatalyst and can be applied in the field of energy conversion devices.

This work was supported by "Network Joint Research Center for Materials and Devices: Dynamic Alliance for Open Innovation Bridging Human, Environment and Materials." Research Program H.K. acknowledges financial support by JST ALCA-SPRING Grant JPMJAL1301 and ERCA Environment Research and Technology Development Fund JPMEE RF20212R01, and Y.S. acknowledges financial support by JSPS KAKENHI Grant 20K15087.

Conflicts of interest

There are no conflicts to declare.

Notes and references

- R. Soni, S. Miyanishi, H. Kuroki and T. Yamaguchi, *ACS Appl. Energy Mater.*, 2021, **4**, 1053.
- (a) Y. Lee, J. Suntivich, K. J. May, E. E. Perry and Y. Shao-Horn, *J. Phys. Chem. Lett.*, 2012, **3**, 399; (b) C. Zhou, H. Y. Yuan, P. Hu and H. F. Wang, *Chem. Commun.*, 2020, **56**, 15201; (c) Y. Sugita, T. Tamaki, H. Kuroki and T. Yamaguchi, *Nanoscale Adv.*, 2020, **2**, 171.
- P. C. K. Vesborg and T. F. Jaramillo, *RSC Adv.*, 2012, **2**, 7933.
- (a) W. T. Hong, K. A. Stoerzinger, Y. L. Lee, L. Giordano, A. Grimaud, A. M. Johnson, J. Hwang, E. J. Crumlin, W. L. Yang and Y. Shao-Horn, *Energy Environ. Sci.*, 2017, **10**, 2190; (b) I. Yamada, A. Takamatsu, K. Asai, T. Shirakawa, H. Ohzuku, A. Seno, T. Uchimura, H. Fujii, S. Kawaguchi, K. Wada, H. Ikeno and S. Yagi, *J. Phys. Chem. C*, 2018, **122**, 27885.
- Y. Sugawara, K. Kamata, A. Ishikawa, Y. Tateyama and T. Yamaguchi, *ACS Appl. Energy Mater.*, 2021, **4**, 3057.
- (a) K. Sugahara, K. Kamata, S. Muratsugu and M. Hara, *ACS Omega*, 2017, **2**, 1608; (b) S. Shibata, K. Sugahara, K. Kamata and M. Hara, *Chem. Commun.*, 2018, **54**, 6772; (c) Y. Sugawara, K. Kamata and T. Yamaguchi, *ACS Appl. Energy Mater.*, 2019, **2**, 956.
- (a) H. Kakizaki, H. Ooka, T. Hayashi, A. Yamaguchi, N. Bonnet-Mercier, K. Hashimoto and R. Nakamura, *Adv. Funct. Mater.*, 2018, **28**, 1706319; (b) I. Yamada, H. Fujii, A. Takamatsu, H. Ikeno, K. Wada, H. Tsukasaki, S. Kawaguchi, S. Mori and S. Yagi, *Adv. Mater.*, 2017, **29**, 1603004; (c) A. Bergmann, I. Zaharieva, H. Dau and P. Strasser, *Energy Environ. Sci.*, 2013, **6**, 2745.
- Y. Sugawara, H. Kobayashi, I. Honma and T. Yamaguchi, *ACS Omega*, 2020, **5**, 29388.
- (a) H. L. Wang and H. J. Dai, *Chem. Soc. Rev.*, 2013, **42**, 3088; (b) X. M. Ge, Y. Y. Liu, F. W. T. Goh, T. S. A. Hor, Y. Zong, P. Xiao, Z. Zhang, S. H. Lim, B. Li, X. Wang and Z. L. Liu, *ACS Appl. Mater. Interfaces*, 2014, **6**, 12684; (c) Q. L. Zhou, Y. P. Ma, X. H. Ma, X. H. Luo, S. Z. Zheng, Y. X. Nan, E. C. Ou, K. D. Wang and W. J. Xu, *Chem. Commun.*, 2020, **56**, 6336.
- D. U. Lee, B. J. Kim and Z. W. Chen, *J. Mater. Chem. A*, 2013, **1**, 4754.
- J. Geng, L. Kuai, E. J. Kan, Q. Wang and B. Y. Geng, *ChemSusChem*, 2015, **8**, 659.
- W. N. Yan, X. C. Cao, K. Ke, J. H. Tian, C. Jin and R. Z. Yang, *RSC Adv.*, 2016, **6**, 307.
- R. Miao, J. K. He, S. Sahoo, Z. Luo, W. Zhong, S. Y. Chen, C. Guild, T. Jafari, B. Dutta, S. A. Cetegen, M. C. Wang, S. P. Alpay and S. L. Suib, *ACS Catal.*, 2017, **7**, 819.
- Y. L. Niu, X. Q. Huang, L. Zhao, W. H. Hu and C. M. Li, *ACS Sustain. Chem. Eng.*, 2018, **6**, 3556.
- B. N. Khiarak, M. Hasanzadeh, M. Mojaddami, S. H. Far and A. Simchi, *Chem. Commun.*, 2020, **56**, 3135.
- A. Grimaud, C. E. Carlton, M. Risch, W. T. Hong, K. J. May and Y. Shao-Horn, *J. Phys. Chem. C*, 2013, **117**, 25926.
- Y. T. Meng, W. Q. Song, H. Huang, Z. Ren, S. Y. Chen and S. L. Suib, *J. Am. Chem. Soc.*, 2014, **136**, 11452.
- (a) K. Dastafkan, Q. Meyer, X. J. Chen and C. Zhao, *Small*, 2020, **16**, 2002412; (b) Y. Wei, C. H. Shin, E. B. Tetteh, B. J. Lee and J. S. Yuo, *ACS Appl. Energy Mater.*, 2020, **3**, 822; (c) Q. C. Xu, H. Jiang, X. Z. Duan, Z. Jiang, Y. J. Hu, S. W. Boettcher, W. Y. Zhang, S. J. Guo and C. Z. Li, *Nano Lett.*, 2021, **21**, 492.
- J. J. Zhang, W. W. Bao, M. Y. Li, C. M. Yang and N. N. Zhang, *Chem. Commun.*, 2020, **56**, 14713.
- (a) Z. Weng, W. Liu, L. C. Yin, R. P. Fang, M. Lo, E. I. Altman, Q. Fan, F. Li, H. M. Cheng and H. L. Wang, *Nano Lett.*, 2015, **15**, 7704; (b) W. Y. Bian, Z. R. Yang, P. Strasser and R. Z. Yang, *J. Power Sources*, 2014, **250**, 196; (c) A. Pendashteh, J. Palma, M. Anderson and R. Marcilla, *Appl. Catal. B-Environ.*, 2017, **201**, 241; (d) R. Z. Jiang, D. R. Baker, D. T. Tran, J. T. Li, A. C. Leff and S. S. Zhang, *ACS Appl. Nano Mater.*, 2020, **3**, 7119.
- M. F. Tovini, A. Hartig-Weiß, H. A. Gasteiger and H. A. El-Sayed, *J. Electrochem. Soc.*, 2021, **168**, 014512.